lubricants

MDPI

Article

Wear Mechanisms in Press Hardening: An Analysis through Comparison of Tribological Tests and Industrial Tools

Jaume Pujante [1,2,*], Eduard Garcia-Llamas [1], Giselle Ramírez [1], Nuria Cuadrado [1,2], Agim Ademaj [3], Montserrat Vilaseca [1] and Daniel Casellas [1,4]

[1] Eurecat, Centre Tecnològic de Catalunya, Unit of Metallic and Ceramic Materials, Plaça de la Ciència 2, 08243 Manresa, Spain; eduard.garcia@eurecat.org (E.G.-L.); giselle.ramirez@eurecat.org (G.R.); nuria.cuadrado@eurecat.org (N.C.); montserrat.vilaseca@eurecat.org (M.V.); daniel.casellas@eurecat.org (D.C.)
[2] Department of Science and Material Engineering, Universitat Politècnica de Catalunya, Av. Eduard Maristany 10-14, 08019 Barcelona, Spain
[3] METAKUS Automotive GmbH, Fehrenberger Straße 1a, 34225 Baunatal, Germany; agim.ademaj@metakus.com
[4] Division of Solid Mechanics, Luleå University of Technology, 971 87 Luleå, Sweden
* Correspondence: jaume.pujante@eurecat.org

Abstract: Press hardened components have become widespread in the automotive industry in structural and crash-resistant applications, thanks to the combination of the complex shapes and high mechanical properties obtained. However, the press hardening of coated boron steel results in severe adhesive-based wear, with tool maintenance being required in as few as 3000 cycles. The current industrial implementation of press hardening is defined to work around this phenomenon. While this aspect has been studied by different authors, most of the literature deals with laboratory-scale tribosimulators, leaving an open question into how this knowledge transfers to macroscopic effects on the industrial process. In this work, wear in press hardening is studied by comparing the results obtained in laboratory conditions with a pilot-scale line, and finally, with wear mechanisms observed on industrial tools. The aim of this study is to consolidate the current knowledge about the micro-mechanisms involved, and to understand to what extent the existing tests reproduce the actual mechanisms observed in the press floor. The results show how material transfer mainly happens as an accumulation of dust compacted into initial defects on the tool surface. Moreover, this mechanism is effectively reproduced in laboratory tribosimulators and pilot environments, showing a similar morphology to wear on industrial tools. The work sheds light on the underlying causes of wear, and its potential mitigation strategies.

Keywords: AlSi-coated boron steel; press hardening; tribology; wear

Citation: Pujante, J.; Garcia-Llamas, E.; Ramirez, G.; Cuadrado, N.; Ademaj, A.; Vilaseca, M.; Casellas, D. Wear Mechanisms in Press Hardening: An Analysis through Comparison of Tribological Tests and Industrial Tools. *Lubricants* **2023**, *11*, 222. https://doi.org/10.3390/lubricants11050222

Received: 25 April 2023
Revised: 8 May 2023
Accepted: 14 May 2023
Published: 16 May 2023

1. Introduction

Press hardening, also known as hot stamping, is a non-isothermal forming process for sheet metals, where forming and quenching take place in the same step [1]. In direct press hardening, blanks are austenitized at a temperature between 900 and 950 °C for 4–10 min in a furnace. The hot blank is then transferred to a set of cooled dies where it is formed in a single stroke. During this step, the cooled dies quench the formed component at a cooling rate higher than 50 °C/s, ensuring a full martensitic microstructure. The total cycle time, including transfer, forming, and quenching, typically takes 15 to 25 s [2].

The use of press hardening allows for the production of lightweight components with very high mechanical properties and complex shapes while avoiding problems such as spring back on the component or damage including fracture on the tools, associated with the cold forming of Ultra-High Strength Steels (UHSSs). For this reason, press hardened components have mainly found uses in structural and crash reinforcement components for the automotive industry [3,4].

The most commonly used press hardening material is aluminized boron steel sheet. This sheet steel is coated with a layer of Al-10%Si with a thickness of between 20 and 36 µm, depending on the specifications [5,6]. During heat treatment, the coating develops a complex sub-layer structure of Al-Si-Fe intermetallic phases plus a metallic Fe-based diffusion layer in the coating–substrate interface. These intermetallics have been reported to be hard and brittle [6–8].

The use of AlSi coated steel sheet offers significant advantages in the direct press hardening process: it prevents decarburization and scaling of the steel sheet, provides barrier corrosion protection [9], and improves component paintability [6].

On the other hand, the presence of the coating dominates tool–workpiece contact during forming, and greatly affects the wear mechanisms observed. The main active wear mechanism appears to be material transfer from the sheet metal coating to the tool. This material accumulates in irregular lumps on the tool surface, which affect component quality [10,11]. The accumulation of the material transfer mechanism is fast and severe, and results in press hardening tools requiring maintenance in the form of re-polishing in as few as 3000 production cycles [12].

Wear in press hardening is a well-researched topic, with relevant contributions coming from different research groups. These contributions often include studies of wear mechanisms using different tribosimulators or laboratory test configurations. Without the intent of compiling a comprehensive list, and following an approximate order of decreasing abstraction, some examples are provided here: Hardell [13] and then Pelcastre [14] used a pin-on-disk reciprocating setup to analyze wear in press hardening, Bruschi and Ghiotti et al. [12] used discontinuous pin-on-disk sliding tests, and Venema et al. [15] presented strip drawing-based simulators, as did later works of Pelcastre et al. [16]. Recent works by Venema [17] and these same authors, Pujante et al. [18], presented semi-industrial tests on omega configurations. All of these experiments obtained remarkably coincident results, identifying a combination of abrasive and adhesive wear mechanisms and proposing the generation of particles from the coating as playing an important role.

However, the analysis of actual press hardening industrial tools is scarce, and this is ultimately needed to verify that the assumed mechanisms and trends are correct. Examples include works such as [19–21], which mainly describe wear features without being yet able to describe the acting micromechanisms.

Filling this gap between laboratory tests and industrial reality is highly interesting. First, it would allow for the development of fundamental knowledge on the actual wear micromechanisms acting in the industrial environment, and understanding to what extent the phenomena observed in laboratory tests translate into the industrial process. Second, it would bring to understanding the relative importances of the different observed mechanisms, and therefore allow for mitigation strategies or solutions to be developed. Finally, it would frame precisely to what extent laboratory tests can be used for the development of these solutions.

In this work, the mechanisms of wear on press hardening tools processing AlSi coated sheet steel are discussed by comparing the wear on actual industrial tools, measured through surface replication, with results from laboratory tribological experiments with two different levels of abstraction: a strip drawing test and an omega tool configuration. An analysis of the results allow for the proposal of a solid extrapolation on how the mechanisms of material transfer act on an industrial process, and to what extent they are reproduced in simplified laboratory setups.

2. Materials and Methods

2.1. Materials

All tests were performed on commercial AlSi-coated 22MnB5 steel sheet. Details on the material format and characteristics are offered for each individual test.

2.2. Evaluation of Coating Mechanical Properties

The mechanical properties of the sub-layers in the AlSi coating were studied at room temperature via nanoindentation, in order to determine the mechanical properties of the individual sub-layers.

Nanoindentation measurements were performed using an XP Nanoindenter (MTS Corp, Oak Ridge Tennessee (EEUU)) equipped with a Berkovich indenter. Samples were analyzed in cross-section and mechanically polished to a mirror surface finish with a 0.05 µm colloidal silica suspension. The indentations were performed at a maximum penetration depth of 200 nm. Hardness values were computed using the Oliver and Pharr methodology [22].

2.3. Strip Drawing Tests

Tool wear was compared to inserts worn in a strip drawing-based tribometer system for press hardening (Figure 1). In this test, sheet metal samples are austenitized in a furnace. The strip is transferred to the strip drawing tool, where it is clamped between two flat tool steel specimens under controlled pressure and pulled by a sled at constant velocity. The frictional force is measured during the test. A detailed description of the test setup can be found elsewhere [23]. While the main aim of this test is to be used to obtain Coefficient of Friction values, it is still a valid reproduction of the tool steel-sheet metal contact in press hardening and its tribological interaction.

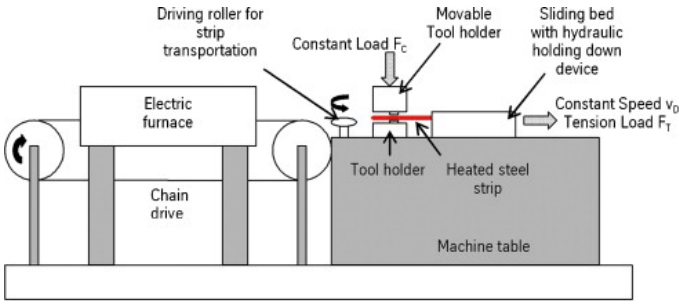

Figure 1. Strip drawing simulator for friction studies in press hardening.

The tool inserts were manufactured from tool steel 1.2367, hardened to 48 ± 1 HRC. The surface of the tool specimens was polished to a roughness Ra of 0.26 µm. The strips of AlSi-coated boron steel were subject to 390 s austenitization at a 900 °C furnace temperature. In these heat treatment conditions, the sub-layer structure in the coating was completely formed [8].

Strips were slid at a velocity of 60 mm/s, while the tool steel inserts were clamped at 6 MPa of pressure. The temperature of the strip at the moment of the beginning of sliding was approximately 800 °C; an average Coefficient of Friction of 0.428 was measured during the sliding test.

The test was repeated five times using the same tool inserts, in order to generate a state of initial wear on the tool steel.

2.4. Pilot Environment: Hot Stamping of Omega Components

A laboratory-scale press hardening line was set up for these trials, aiming to reproduce the main conditions of an industrial environment. Set up of this experimental configuration was discussed in references [18,24]; samples produced in these two references are discussed in the current work.

Heating was performed in a 3 m long continuous roller-hearth convection-radiation furnace, working in an open (oxygen-containing) atmosphere. Austenitized sheets are manually transferred to a 150 t hydraulic press equipped with a set of cooled dies, where hot stamping is performed.

The component geometry was based on an omega-shape (Figure 2), a common concept in press hardening literature. The final geometry was defined based on a survey of cross-section measurements obtained from production B-pillars. The dimensions thus defined were considered to combine a relevant example of the working conditions of industrial tooling with ease of manufacture and inspection. Tool laterals were designed as two symmetrical replaceable inserts. One side was manufactured in commercial hot work tool steel QRO90 heat treated to 50–52 HRC. The other side was left untreated at 36 HRC; a comparison between the two sides may aid in the identification of tribological behavior.

Using this setup, 130 mm × 250 mm, 1.7 mm thick USIBOR 1500 AlSi blanks were stamped with a cycle time of 35 s. Austenitization was performed at 930 °C with a total 360 s furnace time. Tools were measured to reach 80–90 °C at their surface after 25 blanks, assumed as close to steady state. This range of temperatures is representative for industrial press hardening tools.

The campaign discussed in this study spanned 800 cycles, which were divided into several batches. After 270 cycles, replicas of the tools were obtained and analyzed, along with the tool used at the end of production. After the end of the study, one of the lateral inserts was subject to destructive analysis.

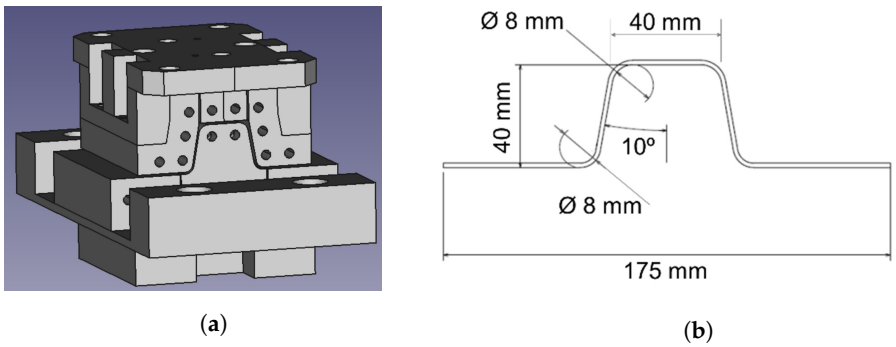

Figure 2. Pilot hot stamping environment. (**a**) Schematic of the tool assembly, including replaceable inserts; (**b**) Component geometry.

2.5. Study of Industrial Tools

Using surface replication, it has been possible to detect and to measure wear on industrial press hardening tools while removing the complications associated with either taking the industrial tool to the lab, or taking dedicated analysis equipment to the industrial environment.

Industrial tools were analyzed at various points of their service life, using production stops to acquire replicas. Details of the tools included in this study are presented in Table 1. Due to production and confidentiality issues, no exact cycle numbers can be given. Instead, order-of-magnitude approximations will be offered for each case. All tools were analyzed in the context of the research project RFCS TestTool.

Table 1. Industrial tools analyzed via surface replication.

Component Produced	Tool Material	Hardness	Sheet Metal Material
B-Pillar	DIN 1.2367	48 HRC	AlSi-coated Boron Steel
B-Pillar	DIN 1.2344	48–50 HRC	AlSi-coated Boron Steel
Frame Dash Panel	DIN 1.2367	48 HRC	AlSi-coated Boron Steel

Surface Replication

Surface replication has been proposed as a methodology for the analysis of wear in industrial production tools [19,21]. In this technique, the surface topographies of the tools are transferred onto a polymeric replica that can be studied in the laboratory without interrupting production. The Accuracy of replication compounds is good enough for the

evaluation of the wear processes, with some formulations showing precisions of better than 0.1 µm, and accuracies of better than 10% [21,25,26].

Replicas were analyzed in the laboratory via optical profilometry techniques, using a Sensofar Plµ 2300 confocal microscope.

3. Results

3.1. Properties of the Al-Si Coating

3.1.1. Micromechanical Analysis of the Coating

AlSi-coated boron steel samples 1.7 mm in thickness were subject to different heat treatments in a convection-radiation furnace. In all cases, the heat treatment consisted in introducing the sample inside the furnace for a set time, followed by extraction and cooling between a pair of steel blocks for an approximate 15 s.

After heat treatment at 900 °C, the coating on the samples, initially metallic Al-Si, developed a microstructure consisting of five sub-layers (Figure 3a). Grigorieva et al. [8] identified the various sub-layers in the system via transmission electron microscopy (TEM). According to [8], the outermost sub-layer (sub-layer 1 in Figure 3a) corresponds to Fe_2Al_5. Sub-layer 2 corresponds to the Al-Si-Fe ternary phase τ_1, sub-layer 3 corresponds again to Fe_2Al_5, and sub-layer 4 to phase τ_1. Finally, a diffusion layer (sub-layer 5) can be observed between coating and substrate, consisting mainly of an iron matrix with $FeAl_3$ inclusions.

In this work, two sets of samples were prepared. The first, under "nominal" conditions, used a furnace temperature of 900 °C and a total furnace time of 390 s. The second was an extremely long furnace time of 1800 s at 900 °C. The aim of this second test was to verify whether changes in the furnace time modify the properties of the sub-layers, or only their relative proportion on the sample.

Nanoindentation studies were performed on cross-sectional samples, as described in Section 2.2. Figure 3a shows a reference image of the indented layers. The hardness results are summarized in Figure 3b.

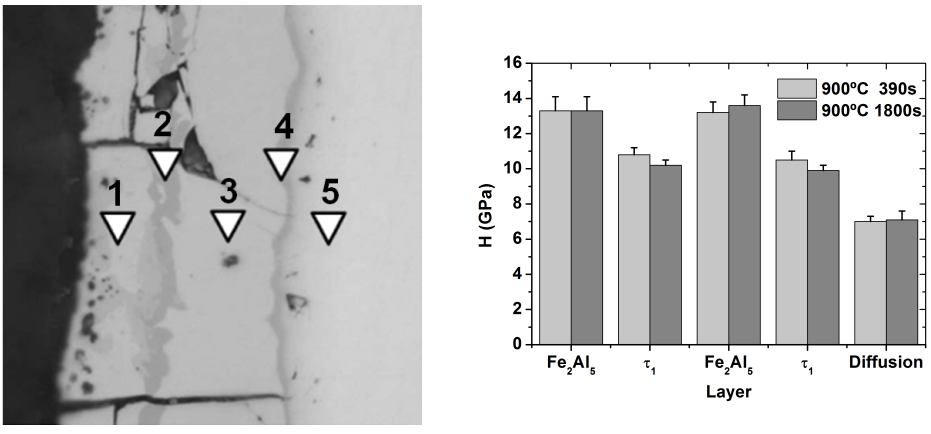

(**a**) (**b**)

Figure 3. Mechanical characterization of the sub-layers of the heat treated AlSi coating. (**a**) Sub-layer structure; triangles indicate the different indented sub-layers identified as follows: (1) topmost Fe_2Al_5, (2) τ_1, (3) Fe_2Al_5, (4) τ_1, (5) Diffusion layer. (**b**) Comparison of hardness of the five layers after different heat treatments.

All layers were much harder than the base heat treated sheet steel, presenting hardnesses of between 7 and 14 GPa. Beginning from the outside of the coating, sub-layers one and three, corresponding to the binary phase Fe_2Al_5, were slightly harder (13 GPa) than layers 2 and 4 (10 GPa), corresponding to the Al-Si-Fe ternary phase τ_1. The outermost part of the diffusion layer (layer 5) showed a lower hardness than the rest of the layers (7 GPa)—approximately in the range of the martensitic 22MnB5 substrate.

This observation agrees with the existing literature, where the coating is reported to be hard and brittle [27]; Pelcastre estimated its overall hardness to be between 511 and 837 HV [14].

It is worth observing that the layer properties did not appear to be modified by the heat treatment, but rather, the hardness was the same for each phase in both of the studied samples. This correlates well to observations from other authors about the phase evolution in AlSi coatings for hot stamping: even though the proportions of the different phases in the coating evolve with time, the chemical composition of each phase remains approximately constant during the process, as discussed in [8], as they are stoichiometric compounds.

Finally, a study was performed to determine the exact properties of the diffusion layer. According to [8], this layer consists mainly of steel with a gradient of aluminum alloyed content. Therefore, it is possible that the properties of the layer are not constant or homogeneous, as they do not correspond to a particular stoichiometric composition.

A detailed analysis of the diffusion layer showed a decrease in hardness inside this layer (Figure 4); an effect also reported by Fan and De Cooman [27]. For the sample subject to the recommended heat treatment, 390 s at 900 °C, an indent located 5 µm under the bottommost τ_1 showed a considerable drop of more than 4 GPa; a 10 µm diffusion layer had been measured for this sample. In the case of a long austenitization sample, 1800 s at 900 °C, a steady decrease in hardness was observed along the 25 µm wide diffusion layer. In this case, a minimum of 3 GPa was found approximately 18 µm under the bottommost τ_1.

This change in mechanical properties could be explained by the diffusion of Al into the Fe-based substrate. In general terms, aluminum is known to adversely affect steel quenchability. The authors Kiani-Rashid and Edmonds [28] observed in a series of dilatometry tests on cast iron that 6.16 % of Al dissolved in a Fe matrix inhibited martensite formation in Fe alloyed with C and Si. In any case, the growth of this diffusion layer is a well known and reported phenomenon. Most relevantly, it is identified as one aspect to control regarding the weldability of the finished products.

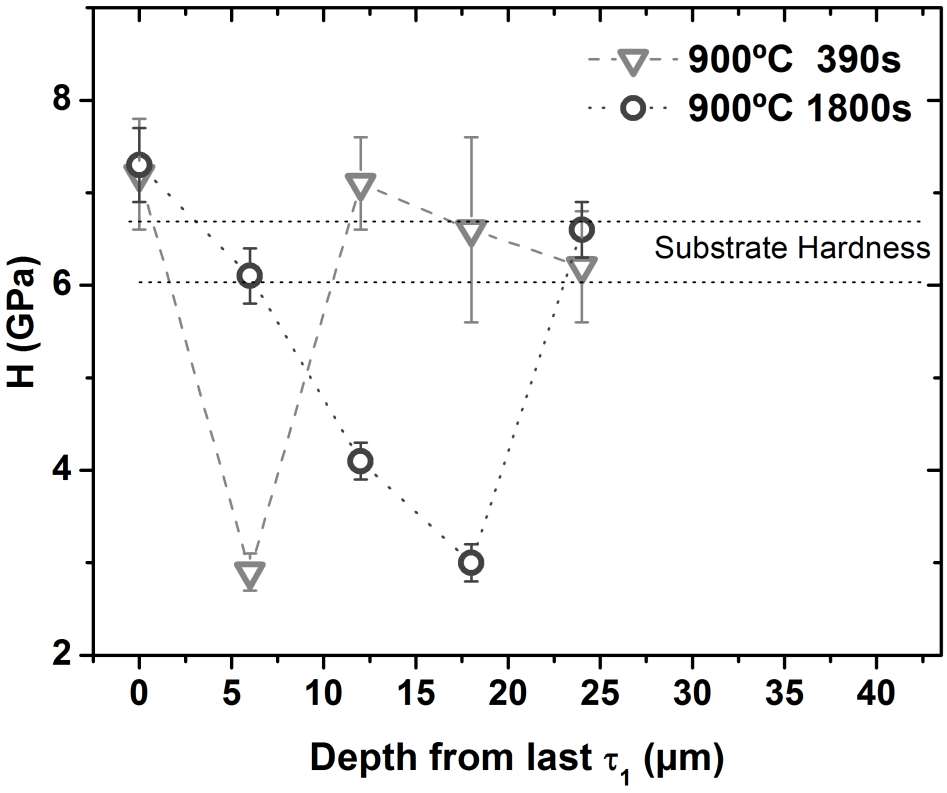

Figure 4. Microhardness profile obtained across the diffusion zone.

3.1.2. Failure of the Coating during Forming

The literature on press hardening reports that adhesion on tools consists of material from the AlSi coating [13,17,19]. The mechanisms through which this material is removed can be related to the properties discussed in the previous section. The coating is formed by intermetallic phases, shows a high degree of hardness, and is reported to be brittle and prone to flaking [27]. This suggests that particles may break off from the coating during forming, generating loose particles that can be then compacted onto the tool.

One cause for this can be friction: the forces and pressures involved in tool-sheet metal sliding can cause particles from the coating to break. This can be clearly seen in the sheet metal used in the strip drawing simulator displayed in Figure 5. When non-slid sections of the sheet metal are observed, the coating is whole and continuous, showing only typical cracks and defects commonly reported for this material (Figure 5a).

However, if a sample slid against the tool steel inserts is analyzed, the coating shows a much worse status, including severe cracking and broken particles (Figure 5b). these mechanisms have been observed and reported by other authors; notably, Ref. [17] observed an almost complete coating removal in slid sheet metal on a tribosimulator drawing radius.

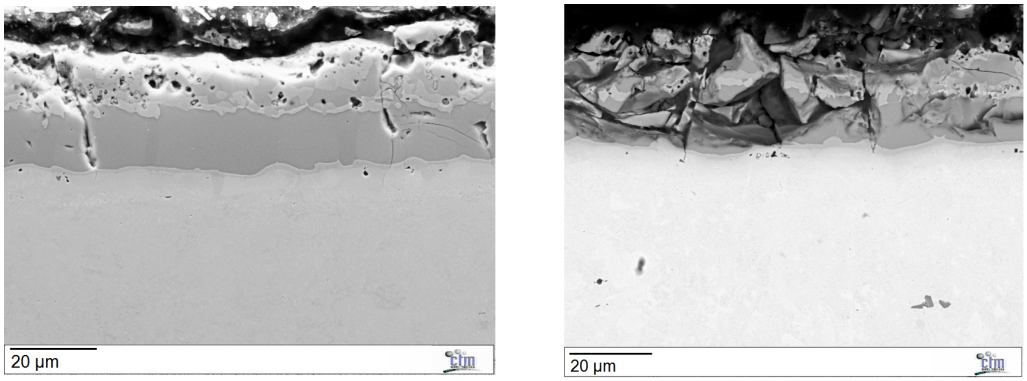

(**a**) (**b**)

Figure 5. Effect of sliding on coating integrity, generated during testing in a strip drawing tribosimulator; (**a**) coating outside the slid zone; (**b**) coating situated on the slid zone, showing severe damage and flaking.

A second mechanism considered in this work is the fracture of the AlSi intermetallic coating when severe plastic deformation takes place on the steel substrate. Qualitatively speaking, the coating should not be able to accommodate significant length changes. In order to prove this, sheet metal samples have been analyzed from the pilot omega components, analyzing the component radius (Figure 6). It could be observed that cracks form readily on the outside of the radius; these cracks correspond to separations or "gaps" in the coating that cannot elongate to cover the increased length (Figure 6a,b). Similar behaviors have been described by Gui et al. [29] in a study performing tensile tests on this same material. Moreover, in that work, very large deformations caused coating particles to flake off from the surface.

Deformation on the inside of the radius (Figure 6c,d) results in coating material breaking from the surface. It is believed that, subject to sufficient compression, the brittle intermetallic coating flakes to accomodate deformation. These cracks look bright when they are observed on the surface, presumably due to the flaking off of the topmost layers, including surface oxides.

As a general conclusion, these two mechanisms (friction and plastic deformation of the substrate) constitute active mechanisms that can generate coating debris during forming, regardless of further interactions with the tool.

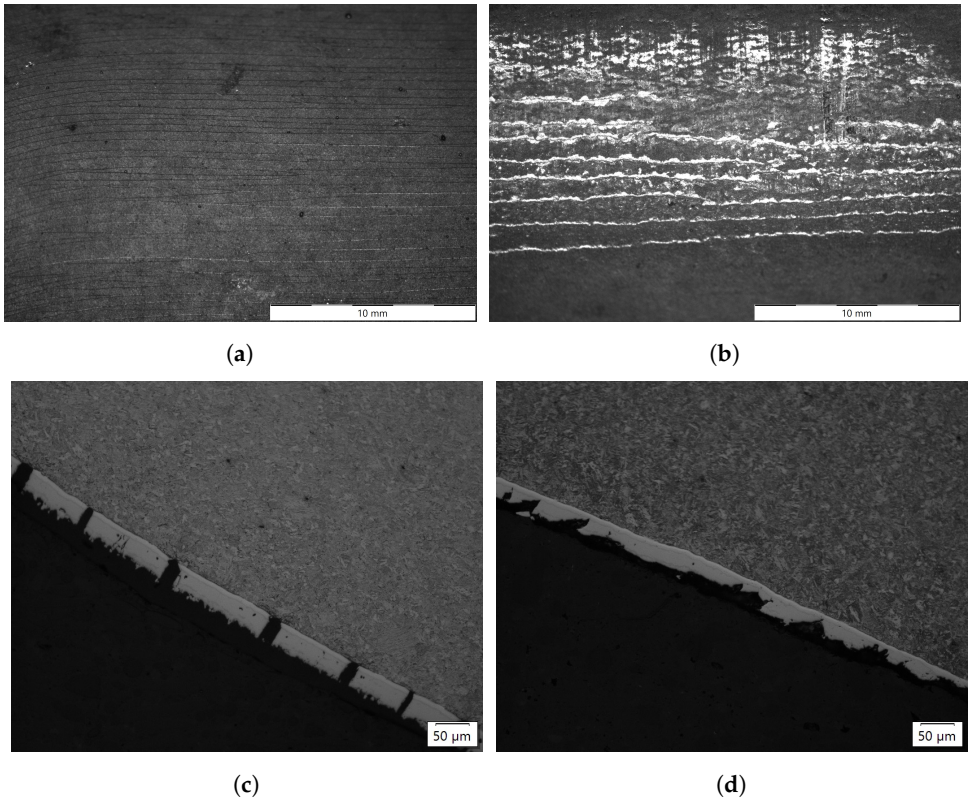

Figure 6. Appearance of cracks on the radius of a formed pilot plant component: (**a**,**c**) 10× stereomicroscopy images of the surface of an external (**a**) and internal (**c**) radii; (**c**,**d**) OM of the cross-sections corresponding to external (**b**) and internal (**d**) radii.

4. Wear Mechanisms on Press Hardening Environments

4.1. Wear on Strip Drawing Inserts

Strip drawing inserts already show the initiation of wear, despite the low amount of material processed in the test. An overview of the inserts, seen in Figure 7, shows a patch of irregular adhesion on the center of the sample, surrounded by abrasive wear tracks.

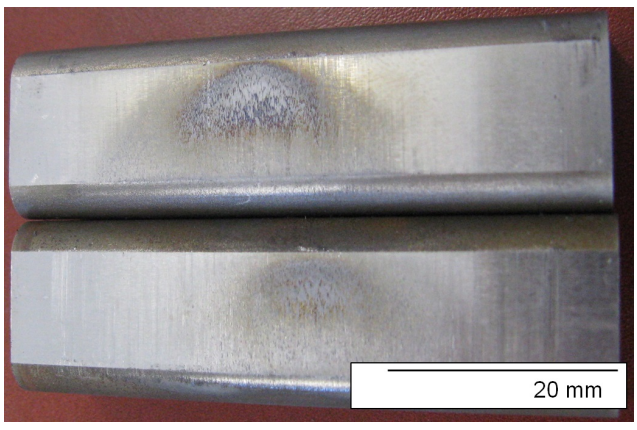

Figure 7. Inserts of the strip drawing facility after testing.

A detailed SEM analysis of the inserts sheds light on the active micromechanisms. First of all, abrasive wear and surface plastic deformation can be observed on the originally polished tool steel (Figure 8a). The appearance of abrasive wear is reasonable, considering that the mechanical analysis of the coating presented in Section 3.1 showed that the hardness of the coating is well above the hardness of the tool steel. In these conditions, sliding under pressure generates material removal and ploughing on the tool steel.

The newly generated grooves appear to act as nucleation points for material transfer, in the form of the compaction of loose dust flaked off from the coating though friction, as was discussed in Section 3.1.2. Figure 8a shows the frontal part of the adhesion patch. Dust can be seen accumulating in this point; moreover, this dust is still at least partially loose on the accumulation side.

Based on this analysis, a mechanism can be proposed where loose debris accumulates on topographical features on the tool surface. As the amount of accumulated dust grows, particles are compacted and partially sintered into a compact layer.

Ultimately, this layer is made of compacted brittle dust, anchored to the tool steel mainly through mechanical means. As a result, the adhesion layer can break off. Figure 8b shows the appearance of the compacted layer at its trailing edge. Cracks can be seen on this zone, showing that the compacted layer is indeed breaking and shedding particles as a result of repeated sliding with the sheet metal.

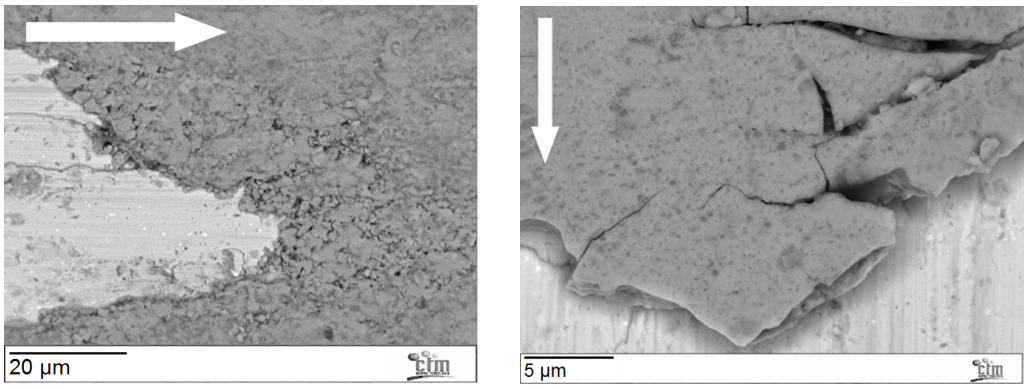

(**a**) (**b**)

Figure 8. Micromechanisms of material transfer on strip drawing inserts; arrow shows sliding direction. (**a**) Accumulation of dust at the front side of the surface features, leading to compaction; (**b**) Fracture of compacts at the rear side. Abrasive wear grooves parallel to the sliding direction can be observed on the bright tool steel surface.

4.2. Wear on Pilot Environment Inserts

After approximately 800 production cycles, tool inserts on the pilot environment showed a complex surface, with different areas where different wear mechanisms dominate. An overview is offered in Figure 9.

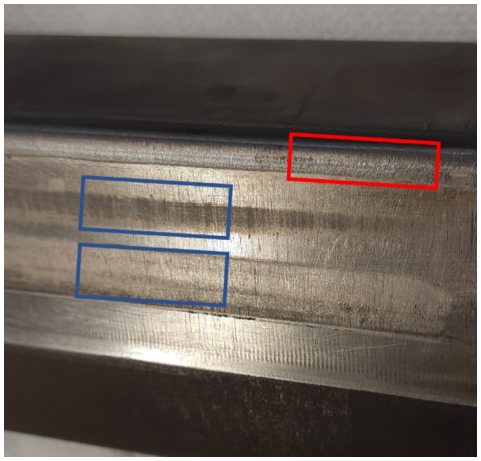

Figure 9. Overview of a pilot environment insert, showing a variety of zones with different wear mechanism combinations: gross material transfer in the drawing radius (red square), fringes of combined wear with sparse material transfer on the tool wall (blue squares), and overall abrasive wear on the rest of the surface.

4.2.1. Gross Material Transfer

Gross material transfer was observed mainly on the drawing radius of the tool (Figure 10). This phenomenon took the shape of thick transfer layers with an homogeneous, almost polished surface. These layers could be recognized thanks to observed rough patches: when analyzed using profilometry, as described in [24], these patches could be confirmed to be holes in the layer. SEM analysis (Figure 10b,c) confirms that the rough surface observed is still transferred material: the patch corresponds to a large flake falling off from the transfer layer, but the fracture takes place inside of the layer itself, and not by dislodging from the original tool surface.

(**a**)

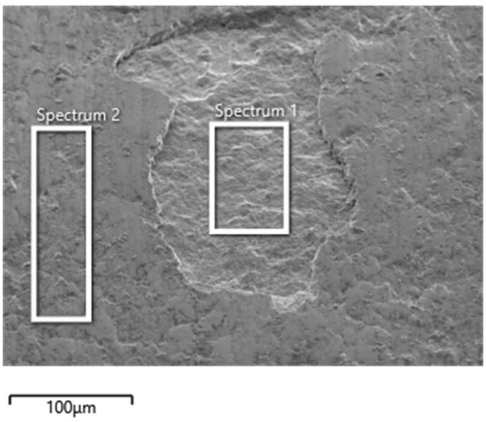

(**b**)

Sample	Al	Si	Fe	O
1	42.78	3.77	42.21	11.24
2	42.22	3.07	41.67	13.04

(**c**)

Figure 10. Material transfer on the drawing radius of the pilot omega tool. (**a**) Overview of the aspect of the radius (photography); (**b**) SEM detail of a rough patch in a polished zone; and (**c**) EDX analysis corresponding to zones 1 and 2.

An overview of the surface through SEM imaging confirms that the tool radius is covered on a compact transfer layer; backscatter electron imaging, offering contrast based on chemical mass, reveals a chemical composition that is clearly differentiated from the tool steel (Figure 11a). The coverage is mostly homogeneous, and only some specific instances can be observed of the bare tool steel showing amid the adhesion. It is worth noticing that this wear state was formed after only 500 production cycles, showing that the material transfer mechanism is extremely active.

Figure 11b shows the front border of this transfer layer, where a combination of wear micromechanisms appear, including plastic deformation, abrasive wear, and the accumulation of debris. This is very similar to the observations in the strip drawing inserts shown in Figure 8 and discussed in Section 4.1, showing that the proposed wear mechanisms of dust accumulation on the surface topography features also fit with the observations in this test configuration.

When observed in cross-section (Figure 11c), this transfer layer is clearly seen to correspond to an accumulation of particles. The morphologies of these particles can be compared to the flakes generated during coating sliding (Figure 5) or severe plastic deformation (Figure 6). Indeed, it appears that the most likely mechanism is the formation of powder and its subsequent accumulation on the tool through geometrical and mechanical means, as opposed to a mechanism of chemical/metallurgical adhesion of the coating on the tool, leading to subsequent coating failure. This is further supported by the fact that no clear welding or transition phase was observed on the adhesion–tool interface: instead, the tool surface appeared to have suffered from a combination of plastic deformation and wear, and the features thus formed acted as anchor points for the transfer material to accumulate.

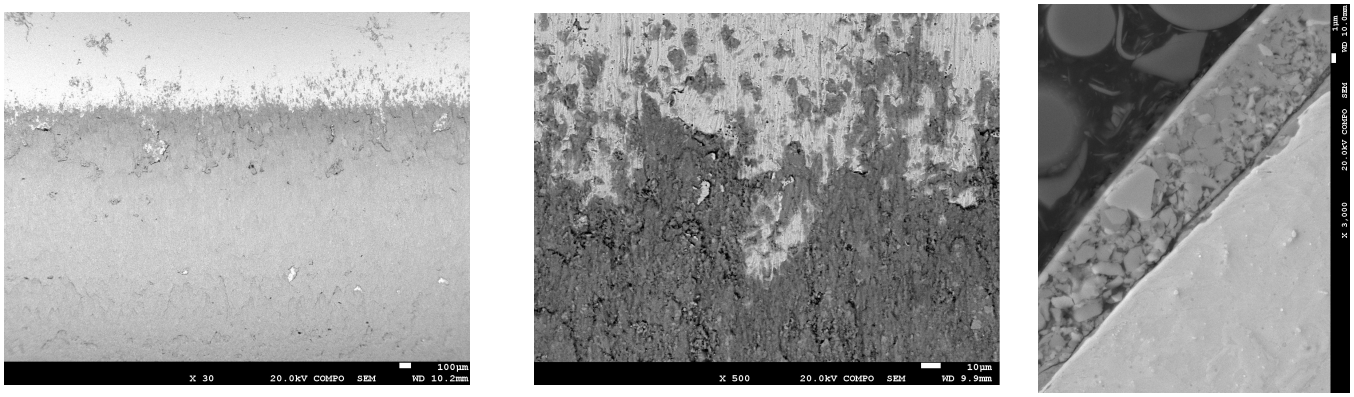

(**a**) (**b**) (**c**)

Figure 11. Surface SEM analysis of the transfer layer on the pilot plant tool radius; sliding direction is top to bottom. (**a**) Overview showing homogeneous coverage of the tool (lighter shade) via compact material transfer (darker shade); (**b**) Upper border of the transfer layer: accumulation of debris, together with mechanical damage on the substrate can be observed; (**c**) Cross-section of the radius, showing a layer of accumulated material.

4.2.2. Abrasive Wear and Plastic Damage

Pilot environment inserts suffer moderate surface damage in the form of abrasion and plastic deformation.

Abrasive wear can appear through two-body micromechanisms, as described by Archard et al. [30], or three-body interaction, and they involve a loss of material on the tool surface. In the case of the studied pilot plant inserts, only mild abrasion is observed. Most interestingly, abrasion marks appear in a clear and obvious way when soft (36 HRC; image in Figure 12a) tool steels are employed in the work referenced in [18]. This clear effect of hardness on the appearance of the mechanism is perfectly consistent with the Archard model, establishing a linear relationship between abrasive wear and hardness.

Even on harder tools, surface damage appears even at very low cycle numbers. As an illustrative example, Figure 13b shows details from the slid surface on a 52 HRC pilot plant tool insert after 500 cycles. Clear evidence can be observed of abrasion on the surface in the form of channels parallel to the top-to-bottom sliding direction. Moreover, a series of ridges and small cracks can be seen, consistent with local plastic deformation generated in an intense contact. Finally, an adhesion of coating particles has begun to form on these ridges, indicating an initiating mechanism for gross material transfer. It must be noticed that these abrasive mechanisms were able to modify the surface roughness of the tool [18,24]. However, they did not result in macroscopic changes to the tool geometry.

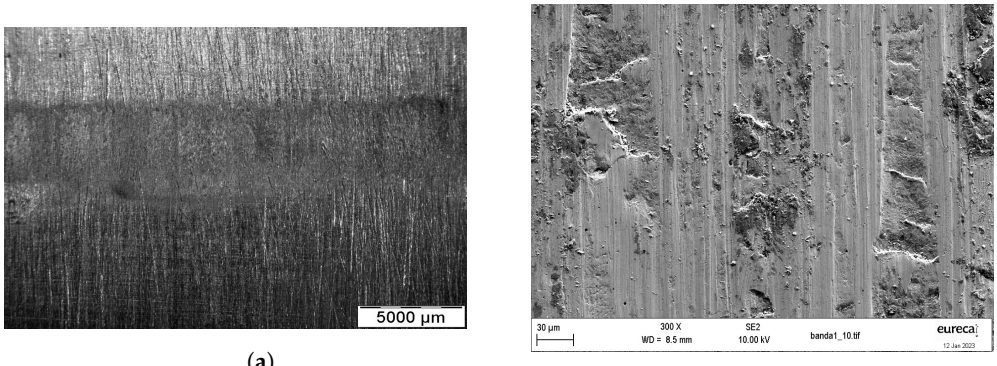

(**a**) (**b**)

Figure 12. Examples of mechanical damage observed in a pilot plant insert: (**a**) wear marks parallel to the sliding direction (top to bottom) on a die wall; (**b**) SEM detail of wear tracks (top-to-bottom sliding lines) and plastic deformation (bumps and ridges in the surface) in this zone.

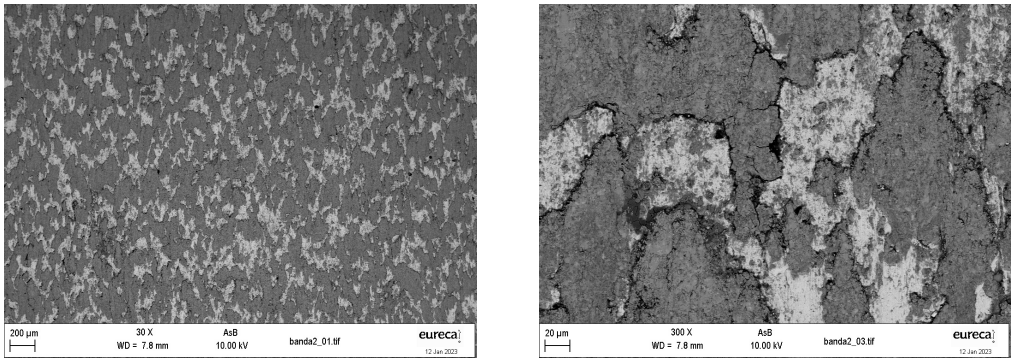

(**a**) (**b**)

Figure 13. Sparse material transfer appearing on fringes on the vertical tool wall; sliding direction is top to bottom: (**a**) SEM overview showing material transfer (dark) on the tool surface (bright); (**b**) Detail of material transfer features.

4.2.3. Combined Wear and Sparse Material Transfer

The flat vertical wall on the omega shape showed horizontal fringes with a matte finish (see Figure 13a). These fringes are reminiscent of material transfer in the strip drawing inserts, consisting of sparse accumulations of material transfer, as opposed to a thick, continuous compact layer.

An SEM analysis of this fringe (Figure 13b) shows a complex combination of wear mechanisms. The tool steel surface is covered on drag marks and plastic deformation, with an appearance that is similar to that described in the previous section. Material transfer takes place on these surface features. In this case, this accumulated material is not as regular as in the radius. First, no significant thickness can be measured via profilometry. Instead, only changes in roughness can be observed. This was discussed in reference [24]. Moreover, the area coverage is not as homogeneous, and the surface appears matted in recognizable individual features, as seen in Figure 13a. Each of these features (Figure 13b) show an appearance that is consistent with an accumulation of dust. Moreover, cracking and fracture are observed on these sparse compacts; again, similar to that observed in the strip drawing inserts (Figure 8).

4.3. Wear on Industrial Tools

4.3.1. Gross Material Transfer on Industrial Tools

As reported in the literature, the tools used in the press hardening of AlSi coated boron steel mainly show adhesive wear-related phenomena, namely, the transfer of material from the workpiece to the tool [21]. The adhered material formed macroscopic features on the tool surface, which could be recognized through naked eye inspection (Figure 14).

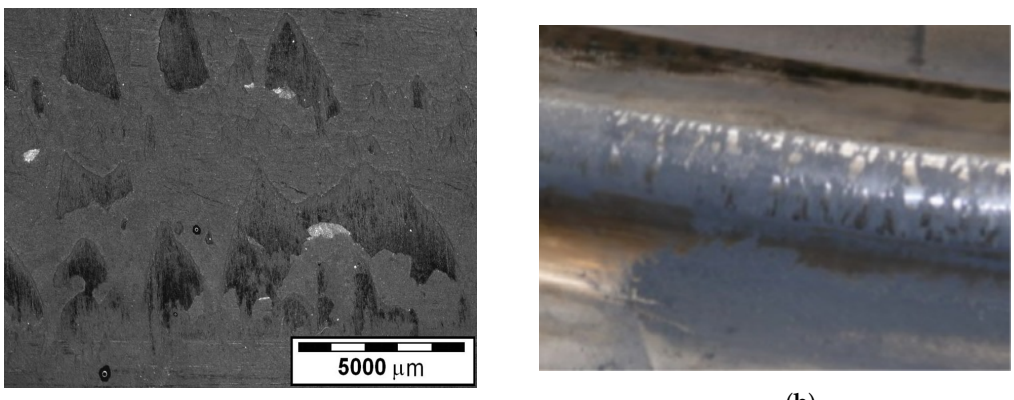

(**a**) (**b**)

Figure 14. Gross material transfer on industrial tools. (**a**) Stereomicroscopy image obtained from a surface replica of a tool radius; (**b**) Picture obtained from a radius of a production tool.

Fragments of adhered material broken off from the tool surface were found entrapped in the replicas, as can be seen in Figure 14a. These particles were hard and brittle, with texture, aspect, and properties similar to compacted powder. Semi-quantitative chemical analysis was performed on these particles via SEM/EDX. All of the particles analyzed showed similar chemical compositions, including primarily aluminum, silicon, and iron (Table 2). This chemical composition roughly corresponds to the coating after heat treatment [6,8]. Based on these results, it is possible to conclude that adhesion in press hardening tools is related to the build-up of material from the coating.

Table 2. EDX analysis performed on samples of adhered dust extracted from a press hardening tool; elements in mass %.

Sample	Al	Si	Mn	Fe
1	37.3	11.9	0.6	41.8
2	45.6	6.1	0.6	44.1
3	36	7	0.7	49.1

4.3.2. Abrasive Wear and Mechanical Damage

Abrasive wear is reported to be a relevant factor in the durability of press hardening tools.

Material transfer imposes a tight maintenance schedule, requiring the removal of transfer layers in as little as 3000 production cycles [12]. Abrasive wear, on the other hand, implies a loss of tool geometry and eventually leads to a macroscopic loss in tool shape, leading to insufficient tool–workpiece contact and a consequent loss in cooling and tolerances.

Abrasive wear can be observed on a microscopic scale on tools with high roughnesses or machining patterns. In this case, the removal of the asperities takes place as the production cycles accumulate, beginning on the areas of the most intense contact. This was reported in [19] for tools working on uncoated material. In this case, the removal of the asperities takes place as the production cycles accumulate, beginning with the areas of most intense contact (Figure 15).

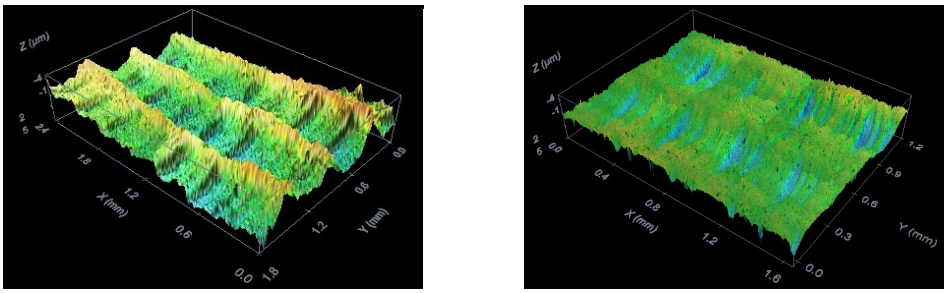

(**a**) (**b**)

Figure 15. Abrasive wear on an industrial press hardening tool. The original surface finish (**a**) has been completely polished away after a production campaign (**b**).

Informal reports from the industry point at cycles of maintenance of approximately 50,000–80,000 cycles, where the tool surface needs to be regenerated via overlay welding on worn spots, and subsequent machining of the surface is needed. A set of production tools could be analyzed using surface replication at the beginning of its production and after approximately 150,000 production cycles. A comparison of the radius profile, presented in Figure 16, shows a considerable loss of macroscopic shape.

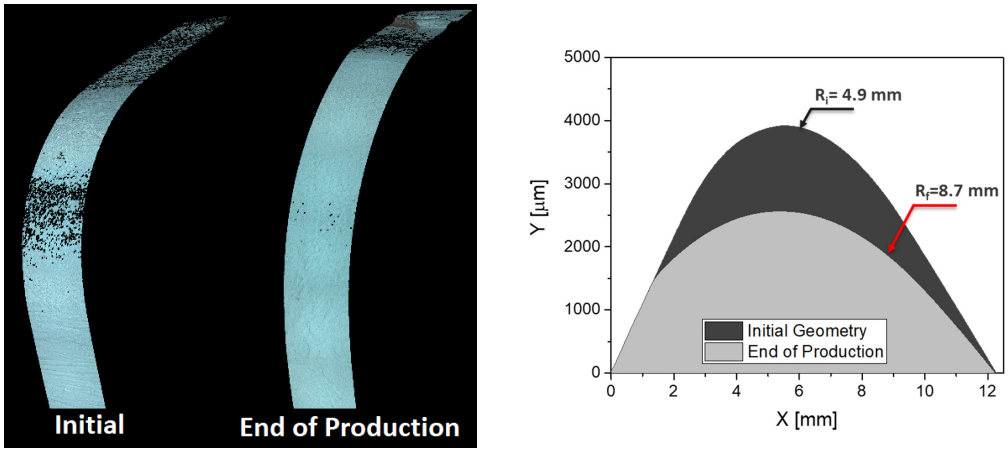

(**a**) (**b**)

Figure 16. Profilometry analysis on a drawing radius from a production tool at the begining and end of production (approx. 150,000 cycles); (**a**) Overview and (**b**) comparison of profiles; please notice that X- and Y axes are not to scale.

4.3.3. Combined Wear and Sparse Material Transfer

Industrial tools show instances of sparse material transfer, with similar morphologies to that observed in the pilot environment. Again, these features appear as matte patches on the tool surface, and they typically appear at some point of the vertical walls in the deep drawing sections.

Destructive analysis of the tools was not possible. Therefore, studies could only be performed indirectly, through the extraction of surface replicas (Figure 17). The overall morphology of this feature is basically equivalent to that in the pilot Environment inserts. When analyzed through confocal microscopy, it can be seen that the rough area of the fringe is formed by discontinuous adhesion lumps, surrounded by bare tool steel with evidence of abrasive wear. An analysis of the surface outside this zone shows an initial smooth surface finish.

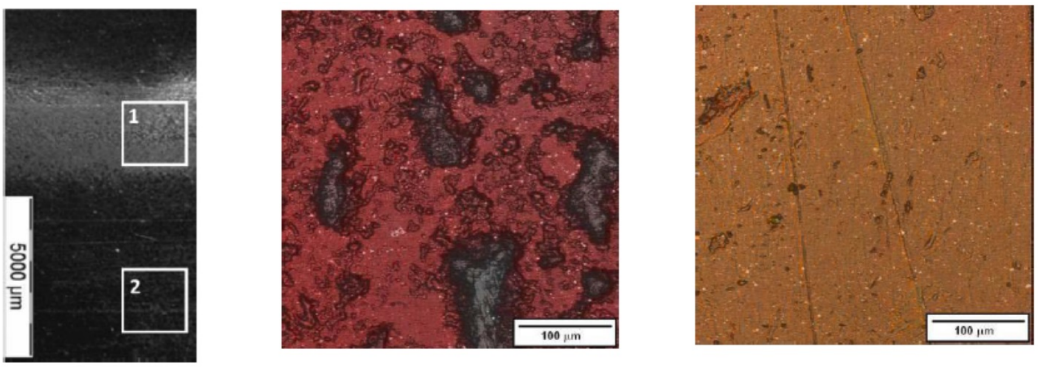

Figure 17. Replica analysis of a combined wear fringe on a vertical wall of an industrial tool.

4.3.4. Ploughing

In the mechanism of ploughing, protrusions on a hard surface interact mechanically with a soft or brittle counterpart during sliding, resulting in the removal of material from the weaker surface. Material thus removed can become loose wear debris, or remain adhered on the asperity (Figure 18). Ploughing is a well known tribological interaction mechanism. Material transfer through ploughing has been reported in the scientific literature for press hardening tribosimulators [31–33].

Ploughing can take place in industrial press hardening tools whenever there are protrusions on the tool steel surface: the locally increased pressure and deformation of the coating results in locally severe tool–component interaction.

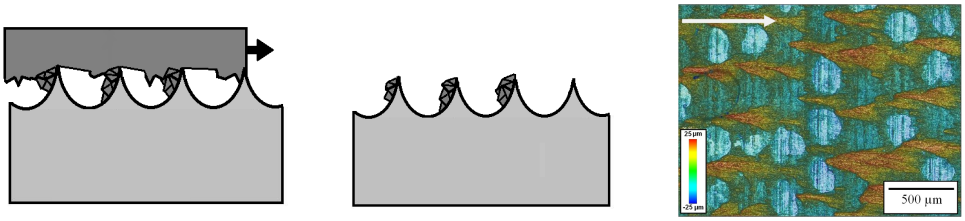

(**a**) (**b**) (**c**)

Figure 18. Mechanism of material transfer through ploughing. (**a**,**b**) Schematic of the micromechanism at work; (**c**) Example of material transfer through plowing observed on an industrial tool with rough surface finish.

Figure 18c shows a relevant example, where material transfer due to ploughing was observed on an industrial press hardening tool with high roughness. In this case, the tool surface showed a machining pattern with a roughness Ra of over 2 µm. Replicas obtained at low cycle numbers from tool walls showed an accumulation of transferred material on the tip of each of the surface finish features. As of 2023, the current trend on industrial press hardening tools is to generate a relatively smooth surface finish precisely to avoid this phenomenon. However, this image is still an illustrative case on how surface features generate material transfer through mechanical means.

5. Discussion

5.1. Material Transfer as the Compaction of Loose Wear Debris

In the mechanism of debris compaction, loose wear debris becomes trapped inside the tool–component contact, and is pressed against irregularities in the tool surface. Due to the high temperatures and the locally high pressures involved, these particles become compacted into a glaze-like layer (Figure 19). This mechanism has been proposed by several authors. Pelcastre et al. [10,33,34] have discussed the important role of dust compaction on the formation of macroscopic material transfer features on press hardening tools via tribological tests in different configurations. Boher [11] also observed in a tribosimulator that macroscopic material transfer takes the form of compacted powder with a morphology and chemical composition that is consistent with the coating particles.

(**a**) (**b**) (**c**)

Figure 19. Mechanism of compaction of wear debris. Given a tool with surface features (**a**), loose debris becomes trapped between the tool and the component during forming, and pressed against these features (**b**), under conditions of pressure and temperature. This leads to further material being consolidated onto the existing feature (**c**).

The results discussed in Section 4 show strong evidence of this mechanism. Powder compaction on the front side of surface features has been directly observed in the strip drawing simulator (Figure 8a) and in the pilot environment (Figures 11 and 13). The resulting macroscopic features have been directly observed for the pilot environment (Figures 11 and 13), including verification through cross-sectional analysis and EDX chemical composition measurement. The observed morphology fits well with the proposed mechanisms in the published literature. Notably, Venema et al. [35] observed very similar results in a strip drawing configuration, including a cross-sectional analysis of transfer layers, with the results being essentially identical to those obtained here. Similar observations were made [17] in a U-shaped stamping tribosimulator resembling the omega

tool configuration used in this work. Material transfer as the mechanical compaction of wear debris is therefore well documented in abstract laboratory tests, and it has also been confirmed to appear in the hot stamping of omega components in this work.

It is reasonable to extrapolate that the same mechanism is taking place on industrial tools. On the one hand, the morphology of the gross material transfer layers is the same as for the industrial tools and the pilot environment; this can be seen by comparing Figures 11 and 14. This is further confirmed through the chemical analysis of particles extracted from the transfer layer in an industrial tool (Table 2, compared to the chemical composition of the transfer layer in the pilot environment (Figure 10c).

The main implication is that in press hardening, the majority of material transfer occurs through geometric and mechanical causes. When severe sliding or plastic deformation occur, dust particles will fall from the coating (see Section 3.1). This mechanism is most intense over the drawing radius, where the two factors are combined. These loose particles will then accumulate onto any geometrical feature, leading to the formation of compacts. While the role of chemical affinity and metallurgical adhesion cannot be completely disregarded, this implies that surface modification leading to reduced affinity will not be able to completely prevent material transfer. This is consistent with observations on [36], where the material transfer during sliding was observed to be governed more by mechanical interaction than by chemical affinity (in that case, in the aluminium-tool steel tribopair).

This observation also offers a possible strategy for reducing the severity of material transfer. By tailoring the properties of the coating at the moment of formation, it may be possible to reduce flaking, and therefore, the amount of dust available to be compacted. In this regard, Kondratiuk et al. [23] reported a decrease in galling at high sliding temperatures. Venema [15] also report differences in the Coefficient of Friction at different sliding temperatures, as do Ghiotti et al. [37] and also Pelcastre et al. [16]. While these works do not offer a common explanation on the specific phenomena, it is still relevant that different setups and test conditions detect differences in friction behavior depending on the sheet temperature.

5.2. Compact vs. Sparse Material Transfer

The difference between compact, gross, and sparse material transfer is highly arbitrary, and is only proposed for the sake of discussion. However, it appears to be relevant that in some cases, material transfer appears in the shape of thick, compact layers, and in others, in sparse lumps with no macroscopic geometrical impact.

Sparse material transfer has been observed on industrial tools since the beginning of the press hardening of coated steel, and it has been reported in investigations concerning industrial tools [19,20]. This feature typically appears as a dull fringe on a flat tool surface, typically at middle-height on deep drawing walls. To this date, detailed observations of these fringes has only been performed through surface replication, as seen in Figure 17. The appearance of these fringes on pilot plant inserts resembling the deep drawing section of a B-Pillar allows them to be studied via SEM, as seen in Figure 13.

Sparse material transfer appears to take place in flat surfaces. This has been observed to be true for industrial tools, but also for pilot tools (Figure 13), and even for tribosimulator inserts (Figure 7). Works in the published literature using flat tribosimulators [16,23,35] also show wear mechanisms that are more similar to this sparse wear. On the contrary, test configurations based on drawing through a radius, such as the work by Boher et al. [11] resulted in thick, compact layers of dust accumulation.The main cause leading to the formation of thick, compact adhesion as opposed to this sparse material transfer appears to be purely geometrical/topological: gross material transfer appears in the radius, while sparse transfer appears on flat surfaces.

While intuitive, the underlying causes for this are not easy to pinpoint. On the one hand, it can be tied to the higher stress, pressure, and intensity of sliding generated by a drawing radius; indeed, increased material transfer has been classically reported, even in cold forming [38]. In the particular case of press hardening, this has been analytically stud-

ied by Deng et al. [39], using an Archard-based phenomenological model that accurately predicted increased material transfer (galling) in the radius of a pilot-scale tool.

On the other hand, the specific system of press hardening introduces an additional factor: the availability of dust to be compacted onto transfer layers. According to Section 3.1, coating particles are generated in higher numbers under intense sliding and plastic deformation, both taking place on a drawing radius: a greater availability of particles to compact will lead to more material transfer.

Finally, as discussed above, the contribution of temperature cannot be discarded. Works in the literature [15,35,40] consistently report on a change in dominant wear mechanisms at different temperatures, with increased "sparse" adhesion at lower temperatures. While this has not been directly observed in this work, it can be noticed that the zones of the omega component where sparse adhesion is observed contact later than the radius, implying a certain loss of temperature in the sheet. The exact reason for this possible change of behavior is unclear, and can be due to changes in the relative hardness levels of tool and coating, leading to different dominances of abrasion, or even to temperature-dependent properties of the coating [35], leading to different dust generation trends.

5.3. Initiation of Material Transfer

It is extremely difficult to design a single experiment that can isolate contributions from mechanical/topological and chemical/adhesive transfer mechanisms in an industry-resembling environment. Therefore, the initiation mechanism for this material transfer cannot be unequivocally demonstrated, but an educated guess can be deduced from the available information.

A discussion on ploughing (Figure 18) reveals how surface features will result in a dramatic acceleration of material transfer mechanisms. While a tool with a smooth surface finish does not offer anchoring points, surface damage mechanisms will quickly generate such features. This has been observed in the strip drawing simulator (Figure 8), where the bare tool steel showed sliding marks. It has also been observed in the pilot environment (Figure 13b), where bare tool steel shows a catalog of sliding damage as well as plastic deformation crimps and cracks.

Works in the literature report similar findings. Pelcastre et al. [16] investigated material transfer in strip drawing tests, performing a cross-sectional analysis of the worn components. Abrasive wear and plastic deformation of the tool surface played a significant role, with transfer layers forming on abrasion grooves, and even generating "intermixed transfer layers" where severe tool plastic deformation resulted in the interlocking of tool steel and material transfer. Similar mixed layer morphology was observed by Venema et al. [35], particulary when sliding at low temperature.

These same authors observed different severities of sparse material transfer when comparing hard (52 HRC) and soft (36 HRC) tool steel QRO90 in a pilot environment, in reference [18]. While micromechanisms could not be explored as the destructive analysis of the tools was not possible at that point, the observations are consistent with a lower degree of hardness leading to more surface damage, and therefore, more initiation points. Notably, this change in surface hardness led to an increased area coverage of sparse adhesion, but not to an increased thickness of material transfer in the vertical tool wall, while gross material transfer in the radius was basically equivalent. The main explanation for this is that a lower hardness leads to an increased amount of material transfer sites, leading to more coverage. On the other hand, the total amount of gross material transfer in a single location once anchor points are formed is governed by the generation of dust, which is most intense in the drawing radius.

This can be contrasted with other tests run in this same configuration by the same authors. In [41], the same pilot test configuration is used to run an 800-cycle production campaign comparing QRO90 and additive manufactured 1.2709 steel, both at an approximate hardness of 50 HRC. The results in that case show very similar sparse wear fringes, despite the significant differences in the chemical compositions of the two steels. Again,

material transfer in the radius is similar in both cases, with thickness occurring in the 400 µm range. Finally, Ref. [24] uses the same configuration to compare QRO90 bare steel to hot work tool steel with a wear-resistant coating. While gross material transfer is mostly equivalent, sparse material transfer is much less severe on the coated tool. In this case, however, the coating itself is a confounding factor. On the one hand, the much harder surface resists abrasive wear and surface plastic deformation, leading to less initiation sites being formed. On the other, however, the coating is explicitly designed as an anti-adhesion coating, including a carbonaceous top-coat. As no destructive analysis was performed in that occasion, it is impossible to clearly understand which of the two factors contributes the most.

Surface damage leading to material transfer is consistent with discussions in the literature about similar tribosystems. As an example, in [36], it was observed that AlCrN-coated tool steel showed higher chemical-metallurgical adhesion with pure aluminum than bare tool steel. However, in sliding tests, material transfer was more severe for the latter. An observation of the acting micromechanisms showed that oxide particles had generated abrasion grooves on the bare tool steel, where material transfer began via mechanical means. On AlCrN-coated samples, this abrasive wear had not taken place, and material transfer could only happen through smearing of the soft aluminium, leading to thin blobs of smeared material transfer instead of the accumulation of dust.

6. Conclusions

In this work, wear mechanisms appearing in press hardening tools working with AlSi-coated boron steel have been studied by comparing the inspection of industrial tools, with results being obtained through laboratory tribology tests. Observations of these analyses have been compared across the different studied systems, and also with the open literature. The main conclusions which can be drawn are the following:

- The main wear mechanism appearing in the press hardening of AlSi-coated boron steel is material transfer. This material transfer is not only related to chemical interaction, but is also generated via mechanical means. The contribution of the latter is decisive in the growth of macroscopic wear features.
- The coating in AlSi-coated boron steel is hard and brittle, showing hardness levels (up to 14 GPa) that are well above a bare tool steel. Moreover, the heat treatment time does not affect the properties of each individual layer, but only their relative proportions.
- Particles can flake off the coating under different conditions, notably during sliding with an external surface (namely, the tool), or in locations of severe plastic deformation. The natural consequence of this is that drawing radii and slope changes are locations where dust generation will be particularly active.
- The compaction of wear debris from the coating is the main micromechanism resulting in the formation of macroscopic features on industrial tools. This phenomenon can readily occur on nucleation spots on the tool surface, even for those generated by other wear mechanisms. As a consequence, this material transfer is mostly based on mechanical and topological reasons. While it has been largely assumed that chemical affinity plays a role, it has not been possible to demonstrate this in the current work.
- The hard sheet metal coating and particles flaking from it are very aggressive towards the tool steel. Abrasion marks are generated extremely fast when direct sliding under pressure takes place, and local plastic deformation can also be observed. These defects will serve as anchor points for material transfer in the form of the accumulation of dust particles.

A follow-up of these conclusions is that material transfer is inherent in the system, and it will take place as long as the current configuration (alloyed AlSi coating, sliding at high temperature, and the absence of lubrication) is kept. However, at least according to the observations of this work, tweaking some of the aspects of the process will affect the severity of wear.

- Tool roughness needs to be kept to a minimum. This does not only involve a good initial surface finish, but also the means to protect this surface from the aggressive abrasive wear generated by the coating particles.
- Maximizing tool surface hardness should have a beneficial impact. On the one hand, it will slow down macroscopic abrasive wear and a loss of geometry. On the other hand, it will also hamper local abrasion and plastic deformation from creating anchor points for material transfer.
- While chemical adhesion has not been demonstrated in this work, a tool surface with low affinity for the coating will make it easier to dislodge adhesion during maintenance, or even through the cycles.

Ultimately, some aspects are left unanswered and could be the focus of future research. One such topic is the effect of system temperature on the dominance of the different wear mechanisms; while some discussion already exists in the literature, translating these observations into macroscopic behavior would be of great industrial relevance. Finally, this work could not prove the effects of chemical/metallurgical adhesion in material transfer in press hardening. Further research into this topic is of great interest, as it has major implications for the design of solutions to wear in press hardening.

Author Contributions: Conceptualization, J.P.; methodology, J.P., E.G.-L., N.C. and A.A.; validation, J.P.; formal analysis, J.P. and E.G.-L.; investigation, J.P., E.G.-L., N.C., G.R. and A.A.; resources, J.P.; data curation, J.P.; writing—original draft preparation, J.P.; writing—review and editing, E.G.-L., G.R., N.C., A.A., M.V. and D.C.; visualization, J.P., E.G.-L. and G.R.; supervision, J.P. and M.V.; project administration, J.P., M.V. and D.C.; funding acquisition, J.P., M.V. and D.C. All authors have read and agreed to the published version of the manuscript.

Funding: The results were partially obtained within the framework of Retos-Colaboración 2017 Project RTC-2017-6448-4 INNOESTAMP (Innovación en recubrimientos PVD para aplicaciones de estampación en caliente), granted by the Spanish Ministry of Science Innovation and University (Ministerio de Ciencia, Innovación y Universidades). Strip drawing simulator tests and the analysis of industrial tools was mainly performed in the framework of the project TestTool, which received funding from the European Commission Research Fund for Coal and Steel under grant agreement no RFCS-CT-2011-00023.

Data Availability Statement: Not applicable.

Conflicts of Interest: The authors declare no conflict of interest.

References

1. Merklein, M.; Lechler, J. Investigation of the thermo-mechanical properties of hot stamping steels. *J. Mater. Process. Technol.* **2006**, *177*, 452–455.
2. Nagathan, A.; Penter, L. Chapter 7: Hot Stamping. In *Proceedings of the Sheet Metal Forming—Processes and Applications* ; Altan, T., Tekkaya, A., Eds.; ASM International: Detroit, MI, USA, 2012; pp. 153–163.
3. Georgiadis, G.; Tekkaya, A.; Weigert, P.; Weiher, J.; Kurz, H. Investigations on the Manufacturability of Thin Press Hardened Steel Components. *Procedia CIRP* **2014**, *18*, 74–79.
4. Neugebauer, R.; Altan, T.; Geiger, M.; Kleiner, M.; Sterzing, A. Sheet metal forming at elevated temperatures. *CIRP Ann.-Manuf. Technol.* **2006**, *55*, 793–816. [CrossRef]
5. Karbasian, H.; Tekkaya, A. A review on hot stamping. *J. Mater. Process. Technol.* **2010**, *210*, 2103–2118. . atprotec.2010.07.019. [CrossRef]
6. Suehiro, M. Properties of Aluminum-coated Steels for Hot-forming. *Nippon. Steel Tech. Rep.* **2003**, *88*, 16–21.
7. Fan, D. A review of the physical metallurgy related to the hot press forming of advanced high strength steel. *Steel Res. Int.* **2009**, *80*, 241–248.
8. Grigorieva, R.; Drillet, P.; Mataigne, J.M.; Redjaïmia, A. Phase Transformations in the Al-Si Coating during the Austenization Step. *Solid State Phenom.* **2011**, *174–174*, 748–790.
9. Allély, C.; Dosdat, L.; Clauzeau, O.; Ogle, K.; Volovitch, P. Anticorrosion mechanisms of aluminized steel for hot stamping. *Surf. Coatings Technol.* **2014**, *238*, 188–196. . [CrossRef]
10. Pelcastre, L.; Hardell, J.; Prakash, B. Galling mechanisms during interaction of tool steel and Al–Si coated ultra-high strength steel at elevated temperature. *Tribol. Int.* **2013**, *67*, 263–271. [CrossRef]

11. Boher, C.; Roux, S.L.; Penazzi, L.; Dessain, C. Experimental investigation of the tribological behavior and wear mechanisms of tool steel grades in hot stamping of a high-strength boron steel. *Wear* **2012**, *294–295*, 286–295. [CrossRef]
12. Ghiotti, A.; Sgarabotto, F.; Bruschi, S. A novel approach to wear testing in hot stamping of high strength boron steel sheets. *Wear* **2013**, *302*, 1319–1326.
13. Hardell, J. High Temperature Tribology of High Strength Boron Steel and Tool Steels. Ph.D. Thesis, Luleå Tekniska Universitet, Luleå, Sweden, 2009.
14. Pelcastre, L. High Temperature Galling: Influencing Parameters and Mechanisms. Ph.D. Thesis, Luleå University of Technology, Luleå, Sweden , 2013.
15. Venema, J.; Atzema, E.; Hazrati, J.; Matthews, D.; van den Boogaard, T. Modelling of Friction in Hot Stamping. *Procedia Manuf.* **2020**, *47*, 596–601.
16. Pelcastre, L.; Kurnia, E.; Hardell, J.; Decrozant-Triquenaux, J.; Prakash, B. High temperature tribological studies on hardfaced tool steels for press hardening of Al-Si coated boron steel. *Wear* **2021**, *476*, 203728. [CrossRef]
17. Venema, J.; Stache, R.; Kotzian, M. Hot Strip Draw Wear Test and Influence of Tool Material on Adhesive and Abrasive Wear. In Proceedings of the 8th International Conference on Hot Sheet Metal Forming of High-Performance Steel CHS2 2022, Barcelona, Spain, 30 May–2 June 2022 ; Oldenburg, M., Hardell, J., Casellas, D., Eds.; Verlag Wissenschaftliche Scripten: Auerbach, Germany, 2022; pp. 171–178, ISBN 978-3-95735-150-0.
18. Pujante, J.; Garcia-Llamas, E.; Casellas, D. Study of Wear in Press Hardening Using a Pilot Facility. In Proceedings of the 7th International Conference on Hot Sheet Metal Forming of High-Performance Steel CHS2 2019, Luleå, Sweden, 2–5 June 2019; Oldenburg, M., Hardell, J., Casellas, D., Eds.; Verlag Wissenschaftliche Scripten: Auerbach, Germany, 2019; pp. 151–158, ISBN 978-3-95735-104-3.
19. Pujante, J.; Vilaseca, M.; Eriksson, K.; Clobes, J.; Alsmann, M.; Casellas, D. Wear mechanism identification on hot stamping tools. In Proceedings of the 3rd International Conference on Hot Sheet Metal Forming of High-Performance Steel CHS2 2011, Kassel, Germany, 13–16 June 2011; Oldenburg, M., Prakash, B., Steinhoff, K., Eds.; Verlag Wissenschaftliche Scripten: Auerbach, Germany, 2011; pp. 377–384, ISBN 978-3-942267-17-5.
20. Pelcastre, L.; Hardell, J.; Herrera, N.; Prakash, B. Investigations into the damage mechanisms of form fixture hardening tools. *Eng. Fail. Anal.* **2012**, *25*, 219–226. [CrossRef]
21. Vilaseca, M.; Pujante, J.; Ramírez, G.; Casellas, D. Investigation into adhesive wear of PVD coated and uncoated hot stamping production tools. *Wear* **2013**, *308*, 148–154. [CrossRef]
22. Oliver, W.; Pharr, G. An improved technique for determining hardness and elastic modulus using load and displacement sensing indentation experiments. *J. Mater. Res.* **1992**, *7*, 1564–1583. [CrossRef]
23. Kondratiuk, J.; Kuhn, P. Tribological investigation on friction and wear behaviour of coatings for hot sheet metal forming. *Wear* **2011**, *270*, 839–849. [CrossRef]
24. Azkona, I.; Pujante, J.; Garcia-Llamas, E.; Caro, J.; Orrit-Prat, J.; Bonet, R. A Novel PVD Coating for Wear Reduction in Press Hardening Tools. In Proceedings of the 8th International Conference on Hot Sheet Metal Forming of High-Performance Steel CHS2 2022, Barcelona, Spain, 30 May–2 June 2022; Oldenburg, M., Hardell, J., Casellas, D., Eds.; Verlag Wissenschaftliche Scripten: Auerbach, Germany, 2022; pp. 513–520, ISBN 978-3-95735-150-0.
25. Nilsson, L.; Ohlsson, R. Accuracy of replica materials when measuring engineering surfaces. *Int. J. Mach. Tools Manuf.* **2001**, *41*, 2139–2145. [CrossRef]
26. Jonsson, P. Sheet Metal Trimming Dies-Characterisation Methods of Geometry and Surface Topography and Influence on Wear. Diploma Thesis, Chalmers University of Technology, Gothenburg, Sweden, 2010.
27. Fan, D.; de Cooman, B. State-of-the-Knowledge on Coating Systems for Hot Stamped Parts. *Steel Res. Int.* **2012**, *83*, 412–433. [CrossRef]
28. Kiani-Rashid, A.; Edmonds, D. Phase transformation study of aluminium-containing ductile cast irons by dilatometry. *Mater. Sci. Eng. A* **2008**, *481–482*, 752–756. [CrossRef]
29. Gui, Z.X.; Wang, K.; Zhang, Y.S.; Zhu, B. Cracking and interfacial debonding of the Al–Si coating in hot stamping of pre-coated boron steel. *Appl. Surf. Sci.* **2014**, *316*, 595–603. [CrossRef]
30. Archard, J. Contact and Rubbing of Flat Surfaces. *J. Appl. Phys.* **1953**, *24*, 981–988. [CrossRef]
31. Heinrichs, J.; Jacobson, S. The influence from shape and size of tool surface defects on the occurrence of galling in cold forming of aluminium. *Wear* **2011**, *271*, 2517–2524.
32. Menezes, P.; Kishore, S.; Kalias, V. Studies on friction and transfer layer: Role of surface texture. *Tribol. Lett.* **2006**, *24*, 265–273. [CrossRef]
33. Pelcastre, L.; Hardell, J.; Courbon, C.; Prakash, B. Tribological behaviour of Al-Si-coated ultra-high-strength steel during interaction with tool steel at elevated temperatures: Influence of tool steel surface topography parameters on galling. *Proc. Inst. Mech. Eng. Part B J. Eng. Manuf.* **2015**, *229*, 1373–1384. [CrossRef]
34. Pelcastre, L.; Hardell, J.; Prakash, B. Investigations into the occurrence of galling during hot forming of Al–Si-coated high-strength steel. *Proc. Inst. Mech. Eng. Part J J. Eng. Tribol.* **2011**, *225*, 487–498. [CrossRef]
35. Venema, J.; Hazrati, J.; Matthews, D.; Stegeman, R.; van den Boogaard, A. The effects of temperature on friction and wear mechanisms during direct press hardening of Al-Si coated ultra-high strength steel. *Wear* **2018**, *406–407*, 149–155. [CrossRef]

36. Pujante, J.; Vilaseca, M.; Casellas, D.; Riera, M.D. The Role of Adhesive Forces and Mechanical Interaction on Material Transfer in Hot Forming of Aluminium. *Tribol. Lett.* **2015**, *59*, 10. [CrossRef]
37. Ghiotti, A.; Bruschi, S.; Medea, F.; Hamasaiid, A. Tribological behavior of high thermal conductivity steels for hot stamping tools. *Tribol. Int.* **2016**, *97*, 412–422. [CrossRef]
38. Schedin, E. Galling mechanisms in sheet forming operations. *Wear* **1994**, *179*, 123–128. [CrossRef]
39. Deng, L.; Pelcastre, L.; Hardell, J.; Prakash, B.; Oldenburg, M. Numerical investigation of galling in a press hardening experiment with AlSi-coated workpieces. *Eng. Fail. Anal.* **2019**, *99*, 85–96. [CrossRef]
40. Medea, F.; Venturato, G.; Ghiotti, A.; Bruschi, S. Tribological performances of new steel grades for hot stamping tools. *J. Phys. Conf. Ser.* **2017**, *896*, 012047. [CrossRef]
41. Pujante, J.; González, B.; Garcia-Llamas, E. Pilot Demonstration of Hot Sheet Metal Forming Using 3D Printed Dies. *Materials* **2021**, *14*, 5695. [CrossRef] [PubMed]